Journal of Nuclear Materials 398 (2010) 160–164

Contents lists available at ScienceDirect

Journal of Nuclear Materials

journal homepage: www.elsevier.com/locate/jnucmat

Investigations of a zirconia solid electrolyte oxygen sensor in liquid lead

Abu Khalid Rivai [a,*], Minoru Takahashi [b,1]

[a] Department of Nuclear Engineering, Graduate School of Science and Engineering, Tokyo Institute of Technology, N1-18, 2-12-1, O-okayama, Meguro-ku, Tokyo 152-8550, Japan
[b] Research Laboratory for Nuclear Reactors, Tokyo Institute of Technology, N1-18, 2-12-1, O-okayama, Meguro-ku, Tokyo 152-8550, Japan

A B S T R A C T

Investigations of a magnesia-stabilized zirconia solid electrolyte oxygen sensor for oxygen control measurement in liquid lead were carried out. The fluid of Bi/Bi_2O_3 as a reference electrode and a molybdenum wire as a working electrode to detect the output signal of the sensor were used. The Nernst equation was used to estimate the electromotive force (EMF) values theoretically. The temperatures of liquid lead were 500, 550 and 600 °C. The results showed that the injection gas temperatures did not affect the detected EMF, the sensor responded well to quick changes of oxygen activity in liquid lead, and the discrepancy between the measured and theoretical EMF of the oxygen sensor output signal was higher at 500 °C than at 550 and 600 °C.

1. Introduction

Lead and lead–bismuth are prospect materials as a coolant of the lead alloy-cooled fast reactors (LFRs) and a spallation target of the accelerator driven system (ADS) [1–3]. However, the advantages of lead alloys from chemical, physical, thermal–hydraulic and neutronics are accompanied by the corrosiveness characteristics of lead alloys and precipitation of lead oxide [1–3]. An example in the practical reactor, this problem caused the accident of K-27 – the first submarine with a Pb–Bi cooled reactor [4]. Therefore, the critical issues for the utilization of lead alloys in nuclear systems are the compatibility of materials with lead alloys and the inhibition of channel plugging caused by the precipitation of solid lead oxide (PbO) and/or precipitation of dissolved metals such as iron and formation of solid impurities [5,6].

Lead oxide (PbO) precipitation can be prevented by controlling the oxygen potential in the lead alloys lower than the lead oxide formation potential. Nevertheless, oxygen concentration in the lead alloys must be controlled sufficiently to form a protective oxide film on the material surfaces to protect the materials from corrosion attack by lead alloys. Therefore, accurate measurement of oxygen concentration in lead alloys is a key issue in solving the critical issues of the lead alloy nuclear systems development.

Zirconia solid electrolyte type has been proposed as the most promising candidate for the oxygen sensor for controlling oxygen concentration in the lead alloys [7–17]. However, until now performances and characteristics investigations of the oxygen sensor mainly focused on the liquid lead–bismuth environment while in the liquid pure lead have been limited. Zirconia solid electrolyte, which is made from a ceramic and known as zirconium dioxide (ZrO_2), has been widely used in the industries due to its oxygen ion conductivity, low thermal conductivity, high flexibility, tensile strength, and resistance to corrosion. The additives of CaO, MgO, Y_2O_3 and Sc_2O_3 are commonly used to stabilize zirconia [18]. From the thermal expansion coefficients viewpoint, MgO has the highest property among them [18].

Validity of the lab-scale oxygen sensor can be improved if the contact part of the apparatus with lead alloys is made of high corrosion-resistant materials due to the corrosiveness of lead alloys. There is a high possibility that the corrosion and oxides product will affect the measured EMF (electromotive force) due to the deposition of the impurities on the surface of the sensor.

In the present study, magnesia-stabilized zirconia electrolyte oxygen sensor tests were carried out in a pure liquid lead. The oxygen sensor was tested using a high corrosion resistance device in the liquid lead over a wide range of oxygen potentials and operating temperatures. The aim of the present study is to investigate the characteristics of the oxygen sensor in a pure liquid lead at various temperatures and oxygen potentials by comparing the measured EMF with the theoretical EMF which is derived from the Nernst equation.

2. Experiment

2.1. Experimental apparatus

Fig. 1 shows the schematic of the stagnant liquid metal test apparatus. The detail of corrosion test apparatus was already described in Ref. [15]. Lead was contained in the alumina crucible

* Corresponding author. Present address: Nuclear Transmutation Technology Group, J-PARC, Japan Atomic Energy Agency, Tokai-mura, Naka-gun, Ibaraki-ken 319-1195, Japan. Tel.: +81 29 282 6026; fax: +81 29 282 5671.
E-mail addresses: rivai.abukhalid@jaea.go.jp (A.K. Rivai), mtakahas@nr.titech.ac.jp (M. Takahashi).
[1] Tel./fax: +81 3 5734 2957.

0022-3115/$ - see front matter © 2009 Elsevier B.V. All rights reserved.
doi:10.1016/j.jnucmat.2009.10.027

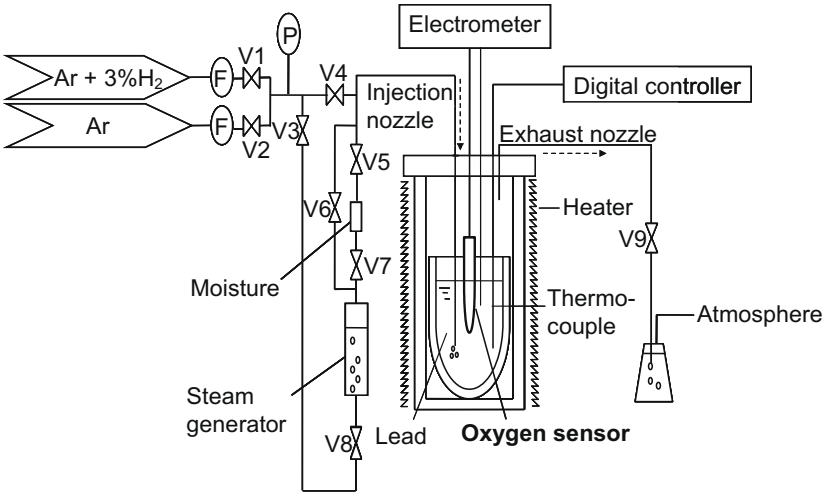

Fig. 1. Schematic of test apparatus.

in the test section with 1250 g in quantity during this experiment. The crucible was 180 mm in length, 60 mm in outer diameter and 5 mm in thickness. The oxygen sensor, molybdenum wire, ceramics nozzle and thermocouple were inserted into lead in the crucible. A contact part of the thermocouple with the liquid lead, the sheath material of which is made of SUS316, was covered by a ceramic tube to protect the thermocouple from corrosion attack by the lead and contamination of the lead because of corrosion products from the thermocouple. The gas injection tube, made of a stainless steel tube, was connected to a ceramic tube in the lead. Therefore, most of the parts in contact with the lead are made of the ceramics materials to prevent impurities in the lead caused by corrosion products of the corrosion test devices.

2.2. Oxygen sensor measurement method

The sensor cell was made from a magnesia-stabilized zirconia ($MgO–ZrO_2$). The internal reference fluid is oxygen-saturated bismuth (Bi: Bi_2O_3 = 95:5 wt%). The sensors were 150 mm in length, 8 mm in outer diameter and 1.5 mm in thickness. The molybdenum working electrode was inserted into the cell to detect the output signal of the sensor. EMF signals were measured continuously by an electrometer with high impedance. The schematic of the oxygen sensor and measurement is shown in Fig. 2.

The oxygen potential in lead can be calculated from the measured EMF using the Nernst equation as follows:

$$E = \frac{1}{2F}\left(\frac{RT}{2}\ln P_{O_2}^{ref} - \frac{RT}{2}\ln P_{O_2}^{melt}\right), \quad (1)$$

where E is the EMF, F is the Faraday constant, R is the gas constant, T is the absolute temperature, and P_{O_2} is the oxygen partial pressure. The oxygen potential in a reference fluid can be calculated by

$$\frac{RT}{2}\ln P_{O_2}^{ref} = \frac{\Delta G^{\circ}_{Bi_2O_3}}{3}, \quad (2)$$

where $\Delta G^{\circ}_{Bi_2O_3}$ is the Gibbs free energy of the Bi_2O_3 formation. The oxygen potential in lead can be calculated by

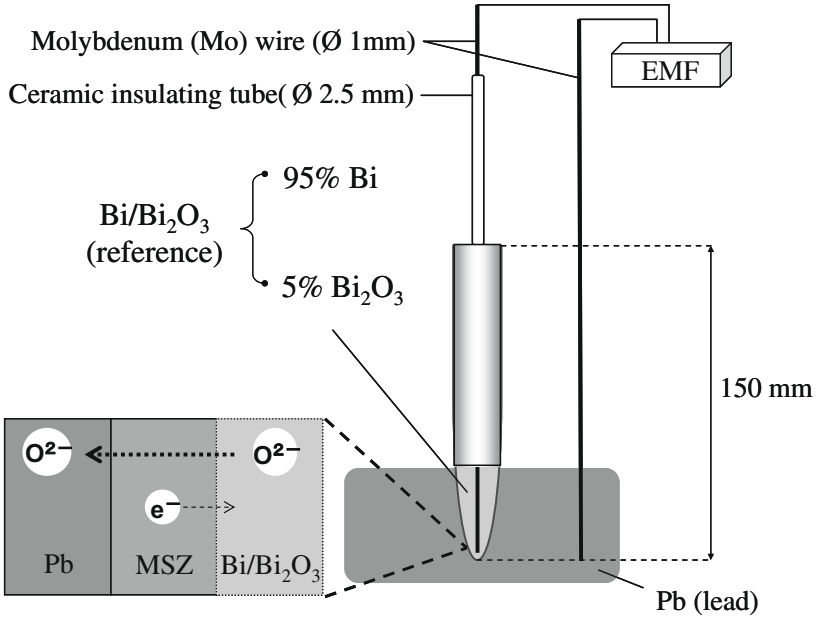

Fig. 2. Schematic of oxygen control measurement.

$$\frac{RT}{2}\ln P_{O_2}^{melt} = \Delta G^{\circ}_{PbO} + RT\ln\left(\frac{C_O}{C_s}\right), \quad (3)$$

where ΔG°_{PbO} is the Gibbs free energy of PbO formation, C_O is the oxygen concentration in the melt, and C_s is the oxygen solubility limit in the melt. The oxygen potential in the injection gas can be calculated by

$$\frac{RT}{2}\ln P_{O_2}^{gas} = \Delta G^{o}_{H_2O} - RT\ln\left(\frac{P_{H_2}}{P_{H_2O}}\right), \quad (4)$$

where $\Delta G^{\circ}_{H_2O}$ is the Gibbs free energy of H_2O formation and P_{H_2}, P_{H_2O} are hydrogen and steam partial pressure in the injection gas. ΔG° and T were calculated in the unit of (J/mol) and (K). The oxygen solubility limit in lead is determined by

$$\log C_s = 3.2 - \frac{5000}{T} \quad [1] \quad (5)$$

for the temperature range of 400–700 °C [1], where C_s is the oxygen solubility in the liquid lead (wt%), T is the temperature of the liquid lead (K). Then, the P_{H_2}/P_{H_2O} ratio can be expressed by

$$\ln\left(\frac{P_{H_2}}{P_{H_2O}}\right) = \left(\Delta G^{\circ}_{H_2O} - \Delta G^{\circ}_{PbO}\right)/RT - \ln C_{O_2} + \ln C_s. \quad (6)$$

Finally, the theoretical EMF can be expressed by,

$$E = \frac{1}{2F}\left[\frac{\Delta G^{\circ}_{Bi_2O_3}}{3} - \Delta G^{\circ}_{H_2O} + RT\ln\left(\frac{P_{H_2}}{P_{H_2O}}\right)\right]. \quad (7)$$

Related to the sensor output signal, it was reported that zirconia electrolytes reveal mixed ionic and electronic conduction when exposed to the high temperatures and low oxygen potentials, and may influence the generation of an EMF signal in the electrochemical cell [19]. Therefore, the sensor output signals have possibly been influenced by this phenomenon. Undoubtedly, the signal response to oxygen becomes larger for better electrical conductivity [20]. However, an exact value for the influence of the mixed ionic and the electronic conduction to the sensor output signal is not estimated in the present study.

2.3. Experimental procedure

The experimental conditions are listed in Table 1. The oxygen sensor was tested in a liquid lead at 500, 550 and 600 °C of temperatures. The oxygen control method using a mixture gas of argon (99.999%Ar), hydrogen (Ar + 3%H_2) and steam was used in this study. As it is shown in the Eq. (4), oxygen potential in the injection gas depends on the hydrogen to steam partial pressure ratio (P_{H_2}/P_{H_2O}). The steam partial pressure was estimated from the measured dew point. The temperature of the water tank for releasing moisture into the gas was controlled. Moisture was added to the mixture gas of Ar and Ar + 3%H_2 by bubbling in the water tank, and then the gas mixture with moisture was injected into the molten lead continuously. Finally, the gas from the test section was continuously exhausted into the atmosphere.

Table 1
Experimental conditions.

Parameters	Conditions
Type of oxygen sensor	MSZ (MgO–ZrO_2)
System pressure	1 x 10^5 N/m^2
Flow rate of injection gas mixture, Ar and Ar + 3%H_2	6.7 x 10^{-7} m^3/s
Velocity of injection gas mixture, Ar and Ar + 3%H_2	5.3 x 10^{-2} m/s
Dew-point temperature	~30 °C
Temperature of dew-point measurement part	~40 °C
Temperature of injection gas mixture	~135 to ~560 °C
Temperature of liquid lead	500, 550 and 600 °C

3. Results and discussion

Output signals of an oxygen sensor in liquid lead are possibly influenced by the injection gas temperature, especially in a short time temperature fluctuation. In case of continuous application, a kind of thermo dynamical equilibrium occurs and sensor output signal is determined by the difference of oxygen potentials between the liquid lead and the bismuth/bismuth oxide reference fluid. In order to clarify the phenomena, the influence of the injection gas temperature on the sensor output signal in a short time range of temperature fluctuation was investigated. Fig. 3 shows the EMF output profile of the sensor at temperature of 600 °C with the injection gas temperature ranging between 135 and 560 °C. First the injection gas temperature was constant at around 560 °C and then suddenly the temperature decreased down to 135 °C. The result showed that the injection gas temperature did not influence the sensor output signal and the control of the oxygen concentration in lead. This happens because the heat capacity of the injection gas was much lower than that of the lead.

The sensor characteristics under the controlled oxygen concentrations in the liquid lead were investigated at the temperature of 500, 550 and 600 °C in the range between 1×10^{-7} and 5×10^{-6} wt% of oxygen concentrations. At first, the oxygen content in the liquid lead was reduced by injecting only Ar + 3%H_2 gas without moisture. Afterwards, the mixture gas of Ar-Ar + 3%H_2-moisture was injected continuously with the calculated value of hydrogen to steam partial pressure. Fig. 4 shows EMF output profiles of the sensor at the temperature of 500 °C. There were two oxygen concentration conditions investigated at this temperature. Firstly, the steam-hydrogen gas was injected with the hydrogen to steam partial pressure ratio (P_{H_2}/P_{H_2O}) corresponding to 5×10^{-7} wt% of oxygen concentration. In the figure the upper line represents the theoretical EMF and the lower line represents the theoretical hydrogen to steam partial pressure ratio. The figure shows that after injection of the gas mixture into the liquid lead the EMF directly decreased, which means the oxygen concentration in the liquid lead increased to about 5×10^{-7} wt%. The EMF output profile shows that the oxygen saturated condition in the liquid lead was reached after about 25 h from the beginning of the gas injection. Afterwards, the hydrogen to steam partial pressure ratio was changed corresponding to 1×10^{-7} wt% of oxygen concentration. The figure shows that the EMF output profile quickly

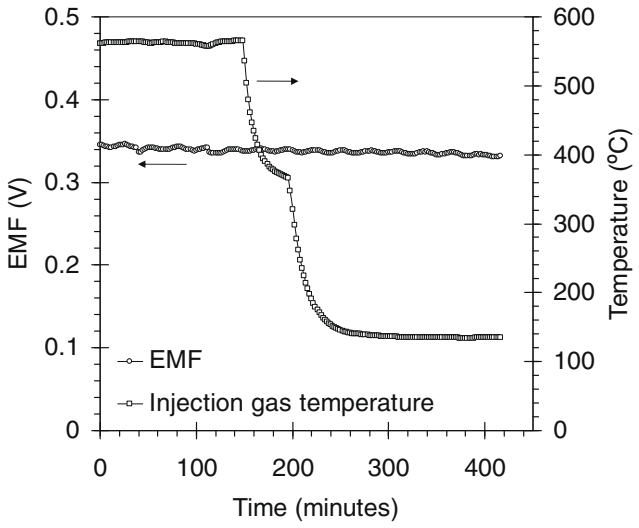

Fig. 3. Comparison of EMF output profile in lead at 600 °C with various injection gas temperatures.

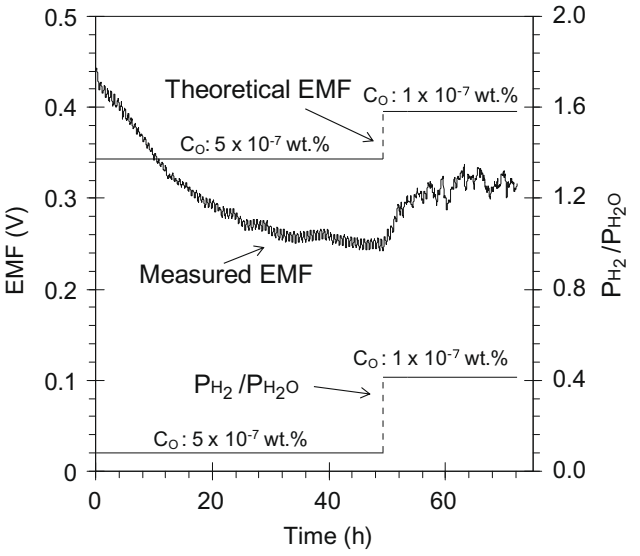

Fig. 4. EMF output profile of the sensor at 500 °C.

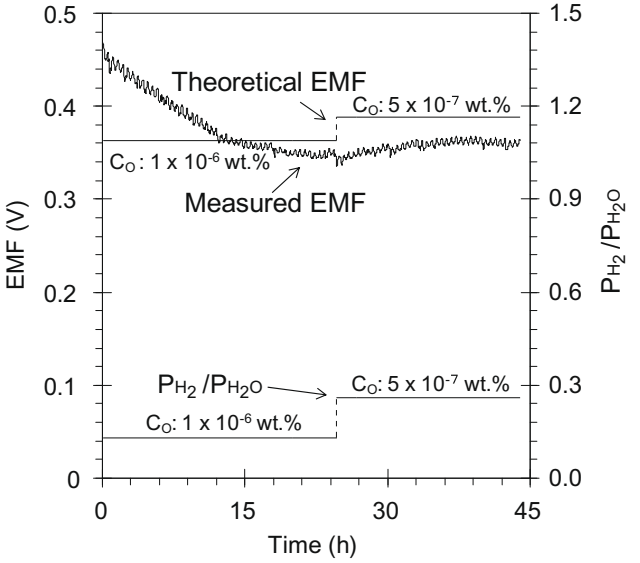

Fig. 5. EMF output profile of the sensor at 550 °C.

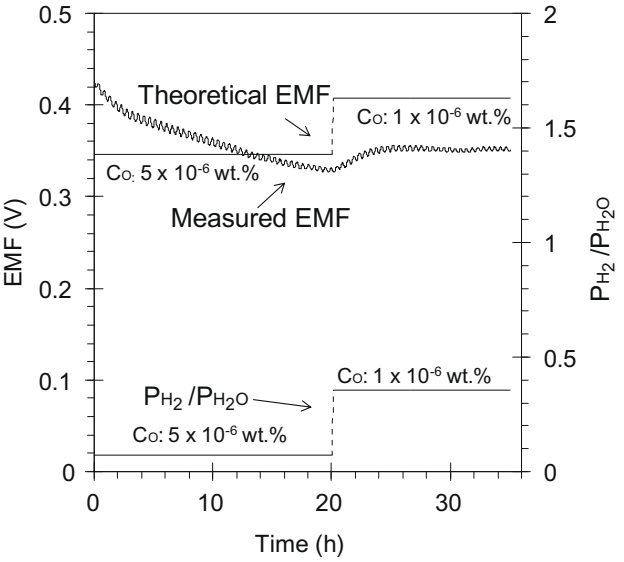

Fig. 6. EMF output profile of the sensor at 600 °C.

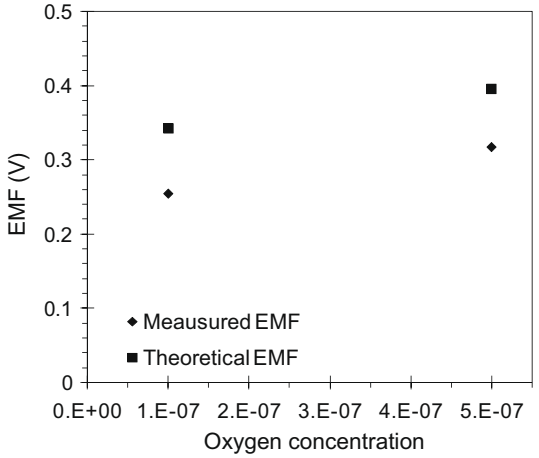

Fig. 7. Comparison of measured and theoretical EMF at 500 °C.

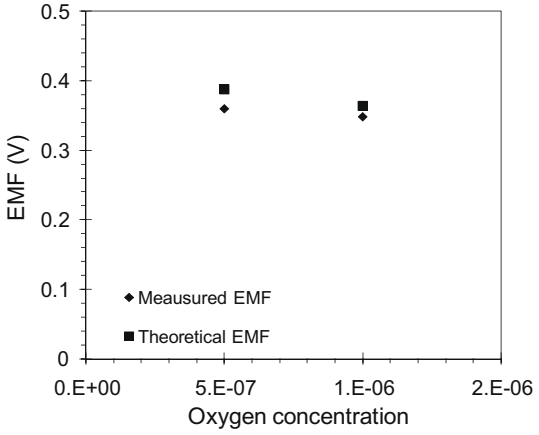

Fig. 8. Comparison of measured and theoretical EMF at 550 °C.

increased due to decrease of oxygen concentration in the liquid lead. The EMF output profile shows a good response time of the sensor when a decrease of oxygen concentration was performed in the liquid lead. Then, oxygen saturation in the liquid lead under this condition was reached after about 15 h. Fig. 5 shows EMF output profiles of the sensor at the temperature of 550 °C with two oxygen concentrations, i.e. 1×10^{-6} wt% and 5×10^{-7} wt%. Similarly the EMF output profile of the sensor at 500 °C, the figure shows that after injection of gas mixture into liquid lead the EMF directly decreased which means the oxygen concentration in lead rose to about 1×10^{-6} wt%. EMF output profiles show that the oxygen saturation condition in the liquid lead was reached after about 19 h from the beginning of the gas injection. Compared with the EMF output profile of the sensor at 500 °C, the oxygen saturation condition at 550 °C (while adding oxygen concentration into the liquid lead) was closer to the value of the theoretical EMF. Afterwards, the hydrogen to steam partial pressure ratio was changed corresponding to 5×10^{-7} wt% of oxygen concentration. The EMF output of the sensor quickly increased while the oxygen concentration in the liquid lead was decreased. Then, the oxygen saturation condition was reached after 15 h from the beginning of the gas

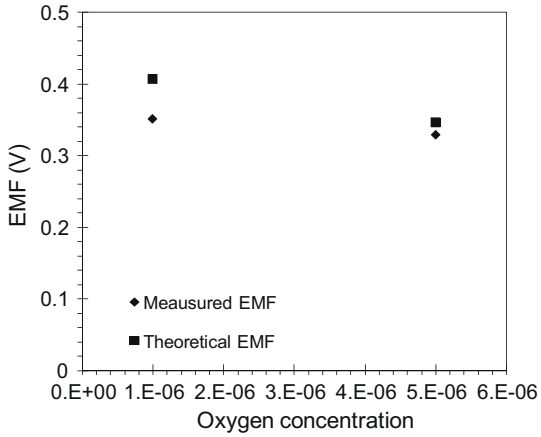

Fig. 9. Comparison of measured and theoretical EMF at 600 °C.

injection. The result shows that the response time of the sensor while oxygen concentration in the lead decrease was satisfactory. Fig. 6 shows EMF output profiles of the sensor at the temperature of 600 °C with two oxygen concentrations, i.e. 5×10^{-6} wt% and 1×10^{-6} wt%. Behavior similar to the EMF output profile of the sensor at 500 and 550 °C was observed. The figure shows that the response time of the sensor while oxygen concentration in the liquid increased and decreased lead at 600 °C was also good.

Figs. 7–9 show the comparison between measured and theoretical EMF at the temperature of 500, 550 and 600 °C, respectively, with various oxygen concentrations. The results showed that there is a discrepancy between the measured EMF and theoretical EMF. There are some reasonable reasons for that discrepancy. Electric conductivity in the oxygen sensor as a ceramic comes from electronic and ionic conduction. The passage of free electrons through the oxygen sensor probe is electronic conduction. Ionic conduction is the transit of ions across point vacancies in the crystal lattice of the oxygen sensor probe. The vacancies are formed by additives of magnesia oxide into ZrO_2. At low temperatures, only a very small amount of ion hopping occurred because the kinetic energy is relatively low. At higher temperatures, which means higher kinetic energy of ions, the vacancies become astir. Then, larger amounts of ion hopping occurred and consequently electric conductivity increases with an increasing temperature. Thus, it is reasonable that the discrepancy between measured and theoretical EMF larger in the case of lead at 500 °C than at the other higher temperatures. It can be predicted that at higher temperatures than the present experiment the discrepancy between measured and theoretical EMF is smaller even negligible. Another reason for the discrepancy is because of the characteristics of the zirconia electrolyte itself [19,20]. Mixed ionic and electronic conduction have possibly occurred in the present oxygen sensor tests and influenced into the oxygen sensor output signals.

4. Conclusions

Investigations of a magnesia-stabilized zirconia solid electrolyte oxygen sensor performance, while applying various oxygen activities in liquid lead at temperatures of 500, 550 and 600 °C were carried out. All the experiments were performed in highly pure lead because the use of the ceramic materials as the gas injection nozzle and the vessel that prevented the formation of impurities in liquid lead. From the investigation and analyses, it can be concluded that:

1. The injection gas temperatures do not affect the detected EMF.
2. The magnesia-stabilized zirconia electrolyte oxygen sensor has good response to quick changes of oxygen activity in liquid lead.
3. There is a discrepancy between the measured and theoretical EMF due to the characteristics of the zirconia electrolyte oxygen sensor. The discrepancy between the measured and theoretical EMF of the oxygen sensor output signal is higher at 500 °C than at 550 and 600 °C.

References

[1] B.F. Gromov, Y.I. Orlov, P.N. Martynov, V.A. Gulevsky, in: Proceedings of Heavy Liquid Metal Coolant (HLMC), 1999, p. 87.
[2] M. Takahashi, H. Sekimoto, K. Ishikawa, T. Suzuki, K. Hata, S. Que, S. Yoshida, T. Yano, M. Imai, in: Proceedings of the 10th International Conference on Nuclear Engineering (ICONE10), Arlington, Virginia, USA, 14–18 April 2002, ICONE10-22226.
[3] P.A. Gokhale, S. Deokattey, V. Kumar, Progr. Nucl. Energy 48 (2006) 91.
[4] P.N. Martynov, A.V. Gulevich, Y.I. Orlov, V.A. Gulevsky, in: The First COE-INES International Symposium (INES-1), October 31–November 4, 2004, Tokyo, Japan, INES1-102.
[5] M. Kondo, M. Takahashi, Progr. Nucl. Energy 47 (2005) 639.
[6] M. Kondo, M. Takahashi, T. Suzuki, et al., J. Nucl. Mater. 343 (2005) 349.
[7] J. Konys, H. Muscher, Z. Voß, O. Wedemeyer, J. Nucl. Mater. 296 (2001) 289.
[8] J.A. Fernández, J. Abellà, J. Barceló, L. Victori, J. Nucl. Mater. 301 (2002) 47.
[9] J.-L. Courouau, P. Trabuc, G. Laplanche, et al., J. Nucl. Mater. 301 (2002) 53.
[10] G. Müller, G. Schumacher, F. Zimmermann, J. Nucl. Mater. 278 (2000) 85.
[11] J. Konys, H. Muscher, Z. Voß, O. Wedemeyer, J. Nucl. Mater. 335 (2004) 249.
[12] J.-L. Courouau, J. Nucl. Mater. 335 (2004) 254.
[13] S. Colominas, J. Abellà, L. Victori, J. Nucl. Mater. 335 (2004) 260.
[14] M. Kondo, M. Takahashi, K. Miura, T. Onizawa, J. Nucl. Mater. 357 (2006) 97.
[15] A.K. Rivai, T. Kumagai, M. Takahashi, Progr. Nucl. Energy 50 (2008) 575.
[16] H.O. Nam, J. Lim, D.Y. Han, I.S. Hwang, J. Nucl. Mater. 376 (2008) 381.
[17] C. Foletti, A. Gessi, G. Benamiti, J. Nucl. Mater. 376 (2008) 386.
[18] Y. Shiratori, F. Tietz, H.P. Buchkremer, D. Stöver, Solid State Ionics 164 (2003) 27.
[19] K. Huang, Y. Xia, Q. Liu, Solid State Ionics 73 (1994) 41.
[20] E. Caproni, F.M.S. Carvalho, R. Muccillo, Solid State Ionics 179 (2008) 1652.